JOURNAL OF PROPULSION AND POWER
Vol. 17, No. 3, May–June 2001

Analysis of Unsteady Blade Row Interaction Using Nonlinear Harmonic Approach

T. Chen,* P. Vasanthakumar,† and L. He‡
University of Durham, Durham DH1 3LE, England, United Kingdom

An efficient nonlinear harmonic methodology has been developed for predicting unsteady blade row interaction effects in multistage axial flow compressors. Flow variables are decomposed into time-averaged variables and unsteady disturbances, resulting in the time-averaged equations with the deterministic stress terms depending on the unsteady disturbances. The nonlinear interaction between the time-averaged flowfield and the unsteady parts are included by a simultaneous pseudotime integration approach, leading to a strongly coupled solution. The rotor/stator interface treatment follows a flux-averaged characteristic-based mixing-plane approach and includes the deterministic stress terms due to upstream running potential disturbances and downstream running wakes, resulting in the continuous nature of all parameters across the interface. The basic computational methodology is applied to the three-dimensional Navier–Stokes equations and validated against several cases. Results show that this method is much more efficient than the conventional nonlinear time-domain methods in modeling the unsteady blade row interaction effects.

Nomenclature

A	=	surface area
e	=	internal energy
$\boldsymbol{F}, \boldsymbol{G}, \boldsymbol{H}$	=	axial, tangential, and radial flux vector
h	=	enthalpy
q	=	heat conduction
r	=	radius
$\boldsymbol{S}$	=	source vector
t	=	time
$\boldsymbol{U}$	=	conservative variable vector
u, v, w	=	axial, tangential, and radial velocities
Vol	=	cell volume
v_{mg}	=	grid moving speed
Y_p	=	blade-to-blade pitch
ρ	=	density
σ	=	interblade phase angle
τ	=	viscous stress components
ω	=	angular frequency

Subscripts

x, θ, r	=	cylindrical polar coordinates

Superscripts

DW	=	downstream of the interface
UP	=	upstream of the interface
$\bar{}$	=	time averaged
$'$	=	unsteady perturbation
$\tilde{}$	=	harmonic amplitude

Introduction

IN the past decade, there have been many investigations on the computation of nonlinear unsteady flows in turbomachinery. Most of these investigations analyze rotor/stator interaction in which the unsteadiness is due to the relative blade motion.[1–7] Some treat unsteadiness due to blade vibration[8,9] or incoming wakes.[10,11] Most of these investigations use the nonlinear time-marching approach to calculate unsteady flows arising from blade row interactions. Despite the increase in the availability of high-speed computational resources, viscous three-dimensional unsteady calculations in a multistage environment still involve substantial computational power. The main complicating factor is the problem of applying periodic boundary conditions for multistage computation in a single blade-to-blade passage domain. Consequently, time-marching methods analyze a multiple-passage domain or the entire annulus in each blade row. Dorney and Sharma[5] proposed the loosely coupled approach by which some reduction in computational effort can be achieved by uncoupling the unsteady interactions between the blade rows. The system of passage-averaged equations formulated by Adamczyk[12,13] included the effect of deterministic periodic unsteadiness on the mean flow through stress terms similar in nature to the Reynolds stresses. Hall[6] combined the mixing plane multistage compressor analysis with the average passage flow modeling and also addressed the problem of closure for various stress correlation terms in the average passage approach by proposing a simple modeling procedure.[7]

The linear unsteady flow modeling in the harmonic frequency domain, on the other hand, offers an efficient approach to the computation of unsteady flows.[14–16] However, the nonlinear interaction between the time-averaged flow and the unsteady disturbances is completely neglected in this approach. Therefore, the focus should be on the development of a method that takes advantage of the computational efficiency of the linear harmonic method while including the nonlinear effects of the time-marching method. In a stimulating framework, Giles[17] combined the idea of Adamczyk[12] with linear unsteady flow modeling to formulate an asymptotic approach in which the level of unsteadiness was the small asymptotic parameter. Unsteady flow was calculated using the linearized form of the unsteady Euler equations assuming that its magnitude was sufficiently small. Changes to the nonlinear steady flowfield due to the time-averaged effect of the linear unsteadiness were introduced through the inclusion of quadratic source terms. He[18] proposed a nonlinear harmonic methodology in which the time-averaged equations with the extra stress terms due to nonlinearity were solved simultaneously with the harmonic perturbation equations in a strongly coupled approach. This method has already been shown to predict flow unsteadiness due to blade flutter with improvement over conventional methods.[19,20] The present work is based on this nonlinear harmonic method to analyze the unsteady blade row interaction governed by three-dimensional Navier–Stokes equations. The deterministic stresses are transferred across the interface of the mixing

Received 3 February 2000; revision received 23 August 2000; accepted for publication 12 September 2000.

*Senior Research Associate, School of Engineering.
†Ph.D. Research Student, School of Engineering.
‡Professor of Thermo-Fluids Engineering, School of Engineering.

plane effecting the continuous nature of all parameters across the interface. Results are provided for two- and three-dimensional cases, demonstrating the prediction capability of the present scheme for blade row interaction effects.

Numerical Approach

Basic Unsteady Flow Governing Equations

The governing equations are the three-dimensional Reynolds averaged unsteady Navier–Stokes equations in cylindrical coordinates (x, θ, r) in an absolute frame of reference. The integral form of the equations is

$$\frac{\partial}{\partial t}\iiint U\,\mathrm{dVol} + \oiint [F\cdot \boldsymbol{n}_x + G\cdot \boldsymbol{n}_\theta + H\cdot \boldsymbol{n}_r]\,\mathrm{d}\boldsymbol{A} = \iiint S\,\mathrm{dVol} + \oiint [F_v\cdot \boldsymbol{n}_x + G_v\cdot \boldsymbol{n}_\theta + H_v\cdot \boldsymbol{n}_r]\,\mathrm{d}\boldsymbol{A} \tag{1}$$

where

$$U = \begin{pmatrix} \rho \\ \rho u \\ \rho v r \\ \rho w \\ \rho e \end{pmatrix} \qquad F = \begin{pmatrix} \rho u \\ \rho u\cdot u + p \\ \rho u\cdot v\cdot r \\ \rho u\cdot w \\ \rho u\cdot h \end{pmatrix} \tag{2a}$$

$$G = \begin{pmatrix} \rho v - \rho\cdot v_{\mathrm{mg}} \\ \rho v\cdot u - \rho u\cdot v_{\mathrm{mg}} \\ [\rho v\cdot v + p - \rho v\cdot v_{\mathrm{mg}}]\cdot r \\ \rho v\cdot w - \rho w\cdot v_{\mathrm{mg}} \\ \rho v\cdot h - \rho e\cdot v_{\mathrm{mg}} \end{pmatrix} \qquad H = \begin{pmatrix} \rho w \\ \rho w\cdot u \\ \rho w\cdot v\cdot r \\ \rho w\cdot w + p \\ \rho w\cdot h \end{pmatrix} \tag{2b}$$

$$S = \begin{pmatrix} 0 \\ 0 \\ 0 \\ \rho v^2/r \\ 0 \end{pmatrix} \qquad F_v = \begin{pmatrix} 0 \\ \tau_{xx} \\ \tau_{x\theta}\cdot r \\ \tau_{xr} \\ u\cdot\tau_{xx} + v\cdot\tau_{x\theta} + w\cdot\tau_{xr} - q_x \end{pmatrix} \tag{3a}$$

$$G_v = \begin{pmatrix} 0 \\ \tau_{\theta x} \\ \tau_{\theta\theta}\cdot r \\ \tau_{\theta r} \\ u\cdot\tau_{\theta x} + v\cdot\tau_{\theta\theta} + w\cdot\tau_{\theta r} - q_\theta \end{pmatrix}$$

$$H_v = \begin{pmatrix} 0 \\ \tau_{rx} \\ r\cdot\tau_{r\theta} \\ \tau_{rr} \\ u\cdot\tau_{rx} + v\cdot\tau_{r\theta} + w\cdot\tau_{rr} - q_r \end{pmatrix} \tag{3b}$$

Time-Averaged Equations

The unsteady flowfield is decomposed into two parts, a time-averaged flow and an unsteady perturbation, for example,

$$U = \bar{U} + U' \tag{4}$$

By substitution of the preceding expression for the conservative variables into the integral form of the unsteady Navier–Stokes equations and by then time-averaging them, the resultant time-averaged equations are given as

$$\oiint [\bar{F}\cdot \boldsymbol{n}_x + \bar{G}\cdot \boldsymbol{n}_\theta + \bar{H}\cdot \boldsymbol{n}_r]\,\mathrm{d}\boldsymbol{A} = \iiint \bar{S}\,\mathrm{dVol} + \oiint [\bar{F}_v\cdot \boldsymbol{n}_x + \bar{G}_v\cdot \boldsymbol{n}_\theta + \bar{H}_v\cdot \boldsymbol{n}_r]\,\mathrm{d}\boldsymbol{A} \tag{5}$$

$$\bar{F} = \begin{pmatrix} \overline{\rho u} \\ \overline{\rho u}\cdot\bar{u} + \bar{p} + \overline{(\rho u)'u'} \\ [\overline{\rho u}\cdot\bar{v} + \overline{(\rho u)'v'}]\cdot r \\ \overline{\rho u}\cdot\bar{w} + \overline{(\rho u)'w'} \\ \overline{\rho u}\cdot\bar{h} + \overline{(\rho u)'h'} \end{pmatrix}$$

$$\bar{G} = \begin{pmatrix} \overline{\rho v} - \bar{\rho}\cdot v_{\mathrm{mg}} \\ \overline{\rho v}\cdot\bar{u} - \overline{\rho u}\cdot v_{\mathrm{mg}} + \overline{(\rho v)'u'} \\ [\overline{\rho v}\cdot\bar{v} + \bar{p} - \overline{\rho v}\cdot v_{\mathrm{mg}} + \overline{(\rho v)'v'}]\cdot r \\ \overline{\rho v}\cdot\bar{w} - \overline{\rho w}\cdot v_{\mathrm{mg}} + \overline{(\rho v)'w'} \\ \overline{\rho v}\cdot\bar{h} - \overline{\rho e}\cdot v_{\mathrm{mg}} + \overline{(\rho v)'h'} \end{pmatrix} \tag{6a}$$

$$\bar{H} = \begin{pmatrix} \overline{\rho w} \\ \overline{\rho w}\cdot\bar{u} + \overline{(\rho w)'u'} \\ [\overline{\rho w}\cdot\bar{v} + \overline{(\rho w)'v'}]\cdot r \\ \overline{\rho w}\cdot\bar{w} + \bar{p} + \overline{(\rho w)'w'} \\ \overline{\rho w}\cdot\bar{h} + \overline{(\rho w)'h'} \end{pmatrix} \qquad \bar{S} = \begin{pmatrix} 0 \\ 0 \\ 0 \\ [\overline{\rho v}\cdot\bar{v} + \overline{(\rho v)'v'}]/r \\ 0 \end{pmatrix} \tag{6b}$$

$$\bar{F}_v = \begin{pmatrix} 0 \\ \bar{\tau}_{xx} \\ \bar{\tau}_{x\theta}\cdot r \\ \bar{\tau}_{xr} \\ \bar{u}\cdot\bar{\tau}_{xx} + \bar{v}\cdot\bar{\tau}_{x\theta} + \bar{w}\cdot\bar{\tau}_{xr} - \bar{q}_x + \overline{u'\cdot\tau'_{xx}} + \overline{v'\cdot\tau'_{x\theta}} + \overline{w'\cdot\tau'_{xr}} \end{pmatrix} \tag{7a}$$

$$\bar{G}_v = \begin{pmatrix} 0 \\ \bar{\tau}_{\theta x} \\ \bar{\tau}_{\theta\theta}\cdot r \\ \bar{\tau}_{\theta r} \\ \bar{u}\cdot\bar{\tau}_{\theta x} + \bar{v}\cdot\bar{\tau}_{\theta\theta} + \bar{w}\cdot\bar{\tau}_{\theta r} - \bar{q}_\theta + \overline{u'\cdot\tau'_{\theta x}} + \overline{v'\cdot\tau'_{\theta\theta}} + \overline{w'\cdot\tau'_{\theta r}} \end{pmatrix} \tag{7b}$$

$$\bar{H}_v = \begin{pmatrix} 0 \\ \bar{\tau}_{rx} \\ \bar{\tau}_{r\theta}\cdot r \\ \bar{\tau}_{rr} \\ \bar{u}\cdot\bar{\tau}_{rx} + \bar{v}\cdot\bar{\tau}_{r\theta} + \bar{w}\cdot\bar{\tau}_{rr} - \bar{q}_r + \overline{u'\cdot\tau'_{rx}} + \overline{v'\cdot\tau'_{r\theta}} + \overline{w'\cdot\tau'_{rr}} \end{pmatrix} \tag{7c}$$

Comparison between the time-averaged equations and the steady form of the original unsteady equations shows that the time-averaging generates extra stress terms in the momentum and energy equations due to nonlinearity, as formulated in the framework by Adamczyk.[12] Nonconservative variables can be worked out from time-averaged conservative variables, for example,

$$\bar{u} = (\overline{\rho u} - \overline{\rho' u'})/\bar{\rho} \tag{8}$$

For the present work, it is assumed that the laminar and turbulent viscosity coefficients are frozen during time averaging, unaffected

by unsteady flows. As a result, the viscous terms are in a linear form except for those concerning the work done by viscous stresses in the energy equations. The standard Baldwin–Lomax mixing length model is used for modeling the turbulence.[21]

Unsteady Perturbation Equations and Harmonic Formulations

The equations for unsteady perturbations can be obtained by the difference between the basic unsteady-flow equations (1) and the time-averaged equations (5). By further assuming that the unsteady perturbations are dominated by the first-order terms, the unsteady perturbation equations can be formed by collecting all of the first-order terms, which gives

$$\frac{\partial}{\partial t}\iiint U'\mathrm{dVol} + \oiint [F'\cdot \boldsymbol{n}_x + G'\cdot \boldsymbol{n}_\theta + H'\cdot \boldsymbol{n}_r]\,\mathrm{d}\boldsymbol{A} = \iiint S'\mathrm{dVol} + \oiint [F'_v\cdot \boldsymbol{n}_x + G'_v\cdot \boldsymbol{n}_\theta + H'_v\cdot \boldsymbol{n}_r]\,\mathrm{d}\boldsymbol{A} \tag{9}$$

Where

$$U' = \begin{pmatrix} \rho' \\ (\rho u)' \\ (\rho v r)' \\ (\rho w)' \\ (\rho e)' \end{pmatrix} \qquad F' = \begin{pmatrix} (\rho u)' \\ \overline{\rho u}\cdot u' + (\rho u)'\cdot \bar{u} + p' \\ [\overline{\rho u}\cdot v' + (\rho u)'\cdot \bar{v}]\cdot r \\ \overline{\rho u}\cdot w' + (\rho u)'\cdot \bar{w} \\ \overline{\rho u}\cdot h' + (\rho u)'\cdot \bar{h} \end{pmatrix} \tag{10a}$$

$$G' = \begin{pmatrix} (\rho v)' - \rho'\cdot v_{\mathrm{mg}} \\ \overline{\rho v}\cdot u' + (\rho v)'\cdot \bar{u} - (\rho u)'\cdot v_{\mathrm{mg}} \\ [\overline{\rho v}\cdot v' + (\rho v)'\cdot \bar{v} + p' - (\rho v)'\cdot v_{\mathrm{mg}}]\cdot r \\ \overline{\rho v}\cdot w' + (\rho v)'\cdot \bar{w} - (\rho w)'\cdot v_{\mathrm{mg}} \\ \overline{\rho v}\cdot h' + (\rho v)'\cdot \bar{h} - (\rho e)'\cdot v_{\mathrm{mg}} \end{pmatrix} \tag{10b}$$

$$H' = \begin{pmatrix} (\rho w)' \\ \overline{\rho w}\cdot u' + (\rho w)'\cdot \bar{u} \\ [\overline{\rho w}\cdot v' + (\rho w)'\cdot \bar{v}]\cdot r \\ \overline{\rho w}\cdot w' + (\rho w)'\cdot \bar{w} + p' \\ \overline{\rho w}\cdot h' + (\rho w)'\cdot \bar{h} \end{pmatrix}$$

$$S' = \begin{pmatrix} 0 \\ 0 \\ 0 \\ [\overline{\rho v}\cdot v' + (\rho v)'\cdot \bar{v}]/r \\ 0 \end{pmatrix} \tag{10c}$$

$$F'_v = \begin{pmatrix} 0 \\ \tau'_{xx} \\ \tau'_{x\theta}\cdot r \\ \tau'_{xr} \\ \bar{u}\cdot\tau'_{xx} + u'\cdot\bar{\tau}_{xx} + \bar{v}\cdot\tau'_{x\theta} + v'\cdot\bar{\tau}_{x\theta} + \bar{w}\cdot\tau'_{xr} + w'\cdot\bar{\tau}_{xr} - q'_x \end{pmatrix} \tag{11a}$$

$$G'_v = \begin{pmatrix} 0 \\ \tau'_{\theta x} \\ \tau'_{\theta\theta}\cdot r \\ \tau'_{\theta r} \\ \bar{u}\cdot\tau'_{\theta x} + u'\cdot\bar{\tau}_{\theta x} + \bar{v}\cdot\tau'_{\theta\theta} + v'\cdot\bar{\tau}_{\theta\theta} + \bar{w}\cdot\tau'_{\theta r} + w'\cdot\bar{\tau}_{\theta r} - q'_\theta \end{pmatrix} \tag{11b}$$

$$H'_v = \begin{pmatrix} 0 \\ \tau'_{rx} \\ \tau'_{r\theta}\cdot r \\ \tau'_{rr} \\ \bar{u}\cdot\tau'_{rx} + u'\cdot\bar{\tau}_{rx} + \bar{v}\cdot\tau'_{r\theta} + v'\cdot\bar{\tau}_{r\theta} + \bar{w}\cdot\tau'_{rr} + w'\cdot\bar{\tau}_{rr} - q'_r \end{pmatrix} \tag{11c}$$

Without loss of generality, the work presented in the rest of the paper considers only one periodic disturbance in a harmonic form:

$$U' = \tilde{U}e^{-i\omega t} \tag{12}$$

The resultant first-order harmonic perturbation equations can be written as

$$\iiint -i\omega\cdot\tilde{U}\,\mathrm{dVol} + \oiint [\tilde{F}\cdot \boldsymbol{n}_x + \tilde{G}\cdot \boldsymbol{n}_\theta + \tilde{H}\cdot \boldsymbol{n}_r]\,\mathrm{d}\boldsymbol{A} = \iiint \tilde{S}\,\mathrm{dVol} + \oiint [\tilde{F}_v\cdot \boldsymbol{n}_x + \tilde{G}_v\cdot \boldsymbol{n}_\theta + \tilde{H}_v\cdot \boldsymbol{n}_r]\,\mathrm{d}\boldsymbol{A} \tag{13}$$

All of the parameters in Eq. (13) are space dependent only because the equations are cast in the frequency domain.

Solution Method

A pseudotime variable t' is introduced to the harmonic perturbation equations, as well as the time-averaged flow equations, as originally proposed by Ni and Sisto.[22] The advantage of introducing pseudotime dependence is that the efficient time-marching integration schemes extensively developed for steady flows can be made use of. Because only the "steady state" is desired for both equations, the multiple-grid technique can be used to accelerate the computations.

The spatial discretization for the equations is the cell-centered finite volume scheme. To suppress numerical oscillations, second- and fourth-order adaptive smoothing is used in streamwise, pitchwise, and radial directions. The pressure sensor in the numerical damping is corrected for the nonlinear effect using an approximate formulation.[18]

Because the time-averaged equations and the unsteady perturbation equations are interdependent, a coupled solution procedure is adopted in the present investigations. The two sets of equations are integrated simultaneously in pseudotime using the four-stage Runge–Kutta scheme. This strong coupling procedure provides high stability that is particularly useful when interaction between time-averaged flow and unsteady perturbations becomes strong. Details about this coupling method can be found in previous papers.[19,20]

Boundary Conditions

Similar to steady method, the nonlinear harmonic method needs only a single blade-to-blade passage domain for a multistage calculation. Boundary conditions are required for inlet, exit, periodic, and solid wall boundaries and for the interface between two blade rows. Two kinds of boundary conditions need to be specified here, one for the time-averaged flow and the other for the harmonic perturbation flow.

For the time-averaged equations, stagnation pressure, stagnation temperature, and flow angles are specified at the stage inlet, whereas static pressure is specified at the stage exit, and local one-dimensional nonreflecting boundary conditions are used. However, a two-dimensional nonreflecting boundary condition, originally proposed by Giles[23] has been implemented on both sides of the inlet and exit at the interface. It has been found necessary when the blade row gap is very small. On the solid wall, the time-averaged velocities are allowed to slip, and an approximate form of the log law is used to calculate the time-averaged wall shear stress.[24] For the harmonic perturbation equations, the phase-shifted periodic condition is implemented at the upper and lower periodic boundaries. The

unsteady perturbation to wall shear stress is obtained by linearizing the approximate log law. Two-dimensional nonreflecting boundary conditions are adopted at both inlet and exit far-field boundaries for the harmonic perturbations.

Rotor/Stator Interface Treatment

At an interface, unsteady disturbances for each blade row are obtained by a Fourier transform of pitchwise spatial nonuniformity of an adjacent blade row. At the inlet to the downstream row, incoming wake perturbations, in terms of velocities (axial, tangential, and radial), pressure, and density, are produced by a spatial Fourier transform of the time-averaged nonuniform field of the outlet from the upstream row. At the outlet from the upstream row, upstream running potential disturbances can be produced by a spatial Fourier transform of the time-averaged nonuniform field at the inlet to the downstream row. All of the upstream and downstream unsteady harmonic disturbances can then be specified in the nonreflecting boundary treatment.

For time-averaged flow, a nonreflecting flux-based approach proposed by Saxer and Giles[25] is adopted. The advantages of this scheme are that it is numerically robust and conserves the total mass, momentum, and energy fluxes across the interface plane accurately. In the present work, the original Saxer and Giles approach has been modified to include the deterministic stresses in the total fluxes due to unsteadiness. The extra stresses due to flow unsteadiness are easily seen as the last terms on both sides of the momentum and energy fluxes [Eq.(14)].

$$\left\{\frac{1}{Y_P}\int \overline{\rho u}\,\mathrm{d}y\right\}^{\mathrm{UP}} = \left\{\frac{1}{Y_P}\int \overline{\rho u}\,\mathrm{d}y\right\}^{\mathrm{DW}}$$

$$\left\{\frac{1}{Y_P}\int [\overline{\rho u}\cdot\bar{u} + \bar{p} + \overline{(\rho u)'\cdot u'}]\,\mathrm{d}y\right\}^{\mathrm{UP}} = \left\{\frac{1}{Y_P}\int [\overline{\rho u}\cdot\bar{u} + \bar{p} + \overline{(\rho u)'\cdot u'}]\,\mathrm{d}y\right\}^{\mathrm{DW}}$$

$$\left\{\frac{1}{Y_P}\int [\overline{\rho u}\cdot\bar{v} + \overline{(\rho u)'\cdot v'}]\,\mathrm{d}y\right\}^{\mathrm{UP}} = \left\{\frac{1}{Y_P}\int [\overline{\rho u}\cdot\bar{v} + \overline{(\rho u)'\cdot v'}]\,\mathrm{d}y\right\}^{\mathrm{DW}}$$

$$\left\{\frac{1}{Y_P}\int [\overline{\rho u}\cdot\bar{w} + \overline{(\rho u)'\cdot w'}]\,\mathrm{d}y\right\}^{\mathrm{UP}} = \left\{\frac{1}{Y_P}\int [\overline{\rho u}\cdot\bar{w} + \overline{(\rho u)'\cdot w'}]\,\mathrm{d}y\right\}^{\mathrm{DW}}$$

$$\left\{\frac{1}{Y_P}\int [\overline{\rho u}\cdot\bar{h} + \overline{(\rho u)'\cdot h'}]\,\mathrm{d}y\right\}^{\mathrm{UP}} = \left\{\frac{1}{Y_P}\int [\overline{\rho u}\cdot\bar{h} + \overline{(\rho u)'\cdot h'}]\,\mathrm{d}y\right\}^{\mathrm{DW}} \tag{14}$$

In the current approach, the deterministic stress terms are conveniently updated using the harmonic amplitudes of unsteady disturbances at both the inlet and exit. The rest of the procedure follows exactly the same way as proposed by Saxer and Giles.[25] These fluxes with unsteady effects are then used to define the flux-averaged flow variables and associated characteristics. Any imbalance in the total fluxes will manifest itself as a jump in the characteristics and will be corrected to ensure the total conservation across the interface in a nonreflecting manner.

Numerical Results

Flat Plate

The first test case is wake/blade interaction in a uniform inviscid steady flow past an unloaded flat plate cascade. The advantage of this configuration is that results can be compared with LINSUB, a widely used linear inviscid analytic program.[26] The flat plate cascade has a pitch/chord ratio of 0.5, stagger angle of 30 deg, and a mean flow Mach number of 0.7. The wake has a pitch that is a factor of 0.9 smaller than the blade, and the flow angle in the wake frame of reference is −30 deg. This result was obtained for a high reduced frequency (based on axial velocity and axial chord) of 13.96 and an interblade phase angle of 400 deg. A very fine computational mesh of 400×50 was used. Figure 1 shows contours of instantaneous entropy throughout the flat plate cascade. Figure 2 shows the comparison of the complex pressure jump distributions between linear harmonic method and LINSUB. Fairly good agreement is obtained for both real and imaginary parts. This test case demonstrates the basic validity of the linear unsteady perturbation solver.

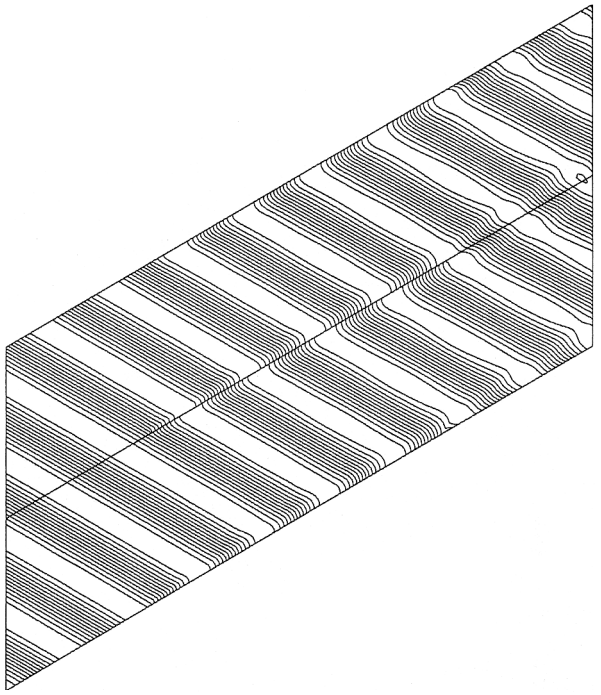

Fig. 1 Contour of entropy in flat plate.

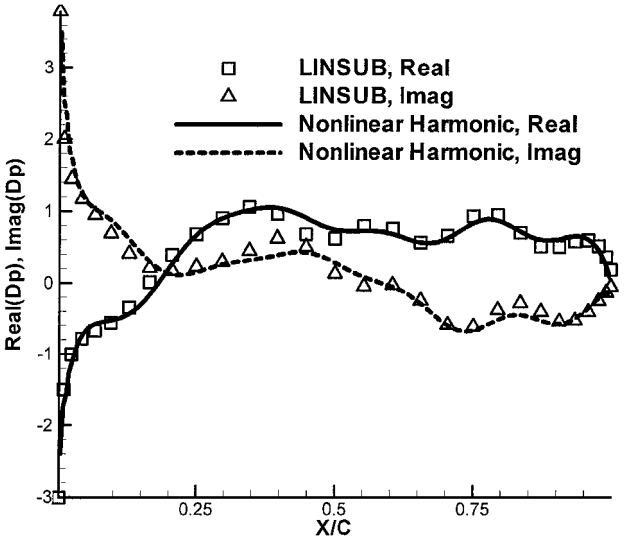

Fig. 2 Complex pressure jump for flat plate.

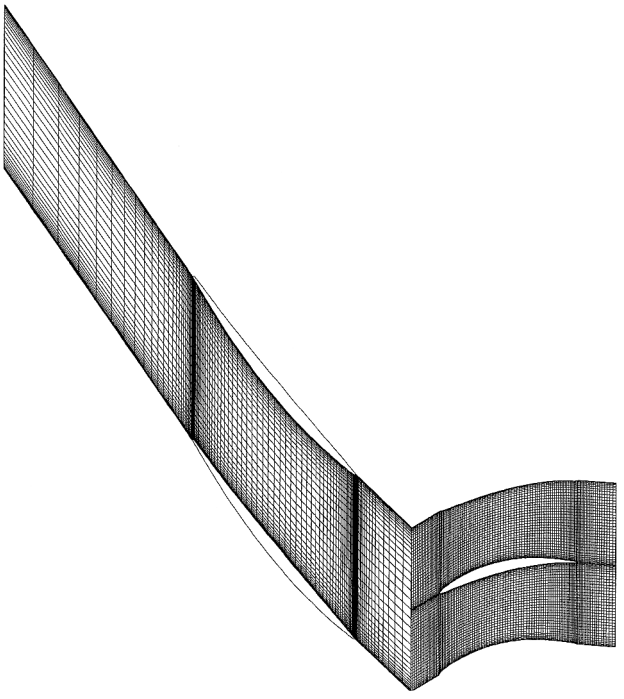

Fig. 3 Two-dimensional mesh for DLR compressor stage.

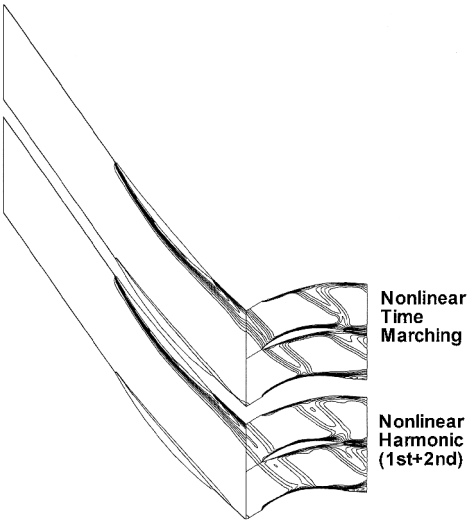

Fig. 4 Entropy contours calculated by nonlinear time marching and nonlinear harmonic (first and second orders).

Two-Dimensional Computation of DLR Compressor Stage

The second test case is a two-dimensional computation of DLR's single stage compressor.[27] It consists of 28 rotor blades of profile R030 and 60 stator blades of profile NACA65. Here the stator blade number is reduced from 60 to 56, giving a blade count ratio of 1 : 2. The validation has been carried out for two different flow conditions, one for transonic flow with a rotating speed of 20,260 rpm and the other for subsonic flow with a rotating speed of 15,000 rpm. Because of space limitations, most of the numerical results are shown for the subsonic flow condition, and only the deterministic stress is shown for the transonic flow condition. A 110×35 mesh for rotor and a 90×35 mesh for stator, shown in Fig. 3, have been used in both subsonic and transonic cases. The mesh at the rotor leading edge has been refined to resolve the local complex flowfield. Considering the temporal accuracy, 200 time steps are adopted in one blade passing period as seen by the rotor.

Figure 4 plots the instantaneous entropy calculated by both the nonlinear time-marching method and the nonlinear harmonic method. With the first two orders of perturbation, the nonlinear harmonic method represents reasonably well the wake passing the interface, propagating downstream. However, its range is slightly thicker than that of the nonlinear time marching. This is acceptable considering that only two orders of wake perturbation are included in the stator. Significantly, the nonlinear harmonic method has captured the physical phenomenon of "wake stretching" inside the stator passage.

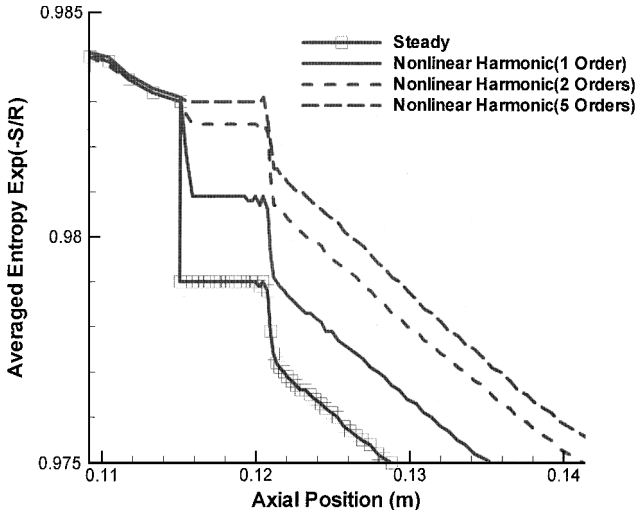

Fig. 5 Mixing loss across the interface by steady method and nonlinear harmonic method with first order, first two orders, or first five orders of wake perturbation.

Figure 5 shows the comparison of mixing losses across the interface between the steady method and nonlinear harmonic method with first order, first two orders, and first five orders of wake perturbation. Loss is expressed in terms of $\exp(-S/R)$, where S is the entropy and R is the gas constant. In steady calculation, only the averaged flux can be transferred at the interface, and the nonuniform wake at the rotor exit is completely mixed out, so nonnegligible mixing loss is generated across the interface. With only first-order wake perturbation, the nonlinear harmonic method can recover nearly half of the mixing loss. With the first two orders of wake perturbation, it can recover about 90% of the mixing loss. However, with the first five orders of wake perturbation, it can recover all of the mixing loss. "Harmonic convergency" has been achieved. This result is consistent with the Fritsch and Giles analysis.[28] On the other hand, the CPU time increases correspondingly by including more orders of harmonic perturbation. The first two orders of harmonic perturbation seems to be the best balance between the cost and accuracy of wake representation.

Because no experimental results for unsteady flows are available, this test is compared with a nonlinear time-marching method. For the nonlinear harmonic method, deterministic stresses can be produced directly from the complex amplitudes. For the nonlinear time-marching method, deterministic stresses are time averaged in one blade passing period seen in the stator. Also, their contributions from first-order unsteady perturbations are produced by temporal Fourier transform. All of the deterministic stresses are nondimensionalized by the inlet dynamic head.

Figure 6 shows that the deterministic stress $\overline{(\rho u)'u'}$ of first-order unsteady perturbation predicted by the nonlinear harmonic method agrees quite accurately with that by the nonlinear time-marching method in the subsonic flow condition. In Fig. 7, the full stress distribution (for the nonlinear harmonic method, it is contributed from the first and second orders) shows a good match between the two methods. Both methods have predicted the trend that the stress is quite nonuniform in the area before the leading edge, mainly due to the strong potential disturbance. Based on the authors' knowledge, there have been no previous results showing this trend.

The nonlinear harmonic method predicts successfully the transport and development of the deterministic stress $\overline{(\rho u)'u'}$ in the

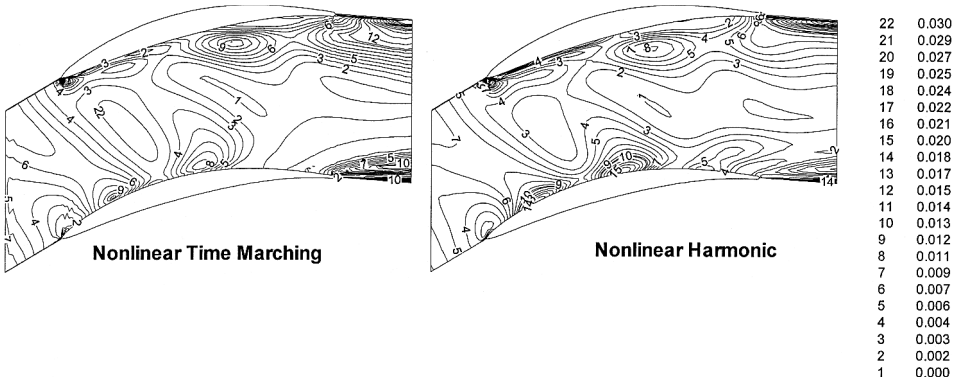

Fig. 6 Deterministic stress $\overline{(\rho u)' u'}$ for DLR stator in subsonic flow condition (first order).

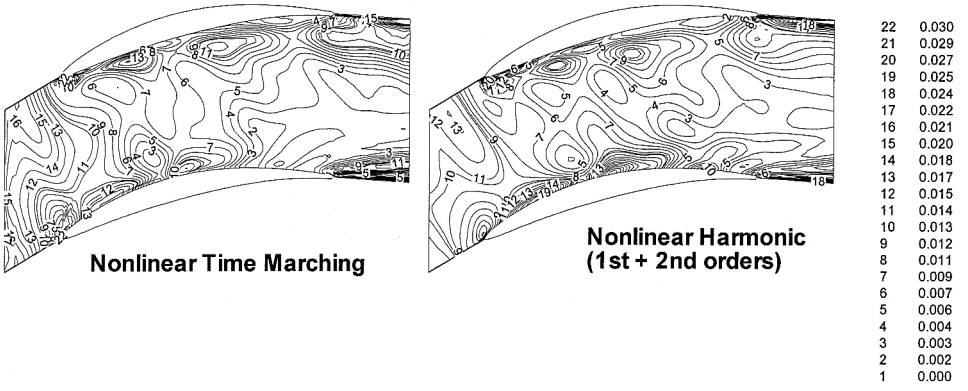

Fig. 7 Deterministic stress $\overline{(\rho u)' u'}$ for DLR stator in subsonic flow condition (full stress).

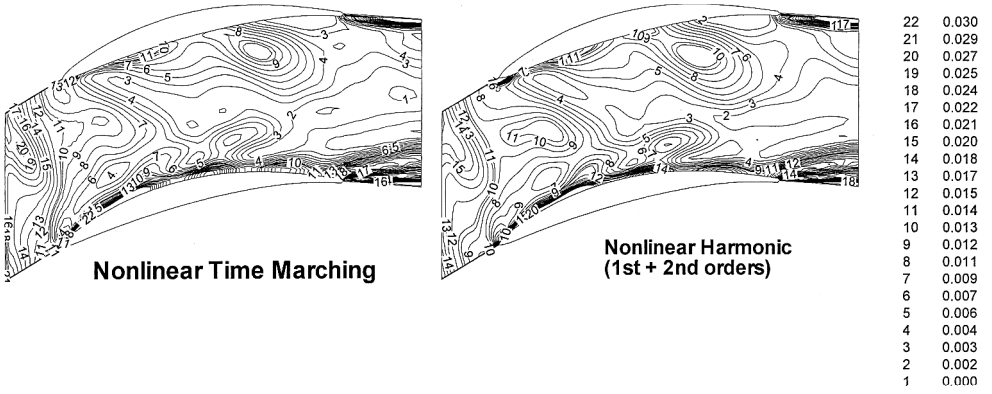

Fig. 8 Deterministic stress $\overline{(\rho u)' u'}$ for DLR stator in transonic flow condition (full stress).

flowfield, and the first two orders of perturbations dominate the deterministic stress, which is consistent with the previous analysis that the first two orders of unsteady perturbations can recover about 90% of the mixing loss. Similar good comparisons have been achieved for all of the other deterministic stresses.

For the transonic flow condition, similar entropy distribution and mixing loss recovery have been demonstrated, but only the distribution of deterministic stress $\overline{(\rho u)' u'}$ is presented in Fig. 8. Consistent agreement between the nonlinear harmonic method and nonlinear time-marching method has been achieved.

Further comparison between the two flow conditions shows that the distribution of $\overline{(\rho u)' u'}$ in the subsonic flow condition (Fig. 7) is quite different from that in the transonic flow condition (Fig. 8). It suggests that the stress distribution depends strongly on the operating condition.

Three-Dimensional Computation of DLR Compressor Stage

The three-dimensional test case is similar to the earlier two-dimensional subsonic case, with a radial mesh of 39 cells. The compressor works in subsonic condition with a mass flow of 13.9 kg/s. Figure 9 shows a side view of the three-dimensional compressor stage. Calculations have been carried out by three methods, namely, steady, nonlinear time-marching, and nonlinear harmonic methods. A multigrid technique has been activated for acceleration in all of the three methods. Both time-averaged and unsteady flowfields of the whole domain have been worked out.

Figure 10 shows the radial distribution of pitch-averaged static pressure across the interface. Steady method generates a pressure jump between the rotor exit (long dash line) and the stator inlet (dash dot line), which is due to the mixing of wake blockage. It is observed that the pressure jump at the lower half is larger than that at the upper half, and it reaches maximum at the height of around 25%. This is because wake blockage is stronger at the lower half, where the vertical interface is nearer to the rotor exit. However, the nonlinear harmonic method produces continuous pressure distribution at the interface. At each height section, the pitch-averaged pressure by the nonlinear harmonic method is lower than that by the steady method.

Deterministic stresses at the midchord plane of the stator have been compared between the nonlinear time-marching and

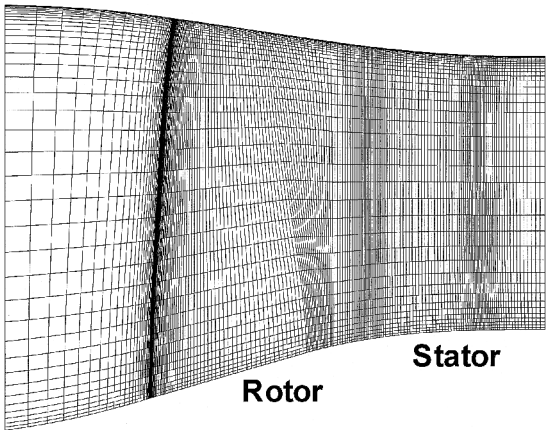

Fig. 9 Side view of DLR compressor.

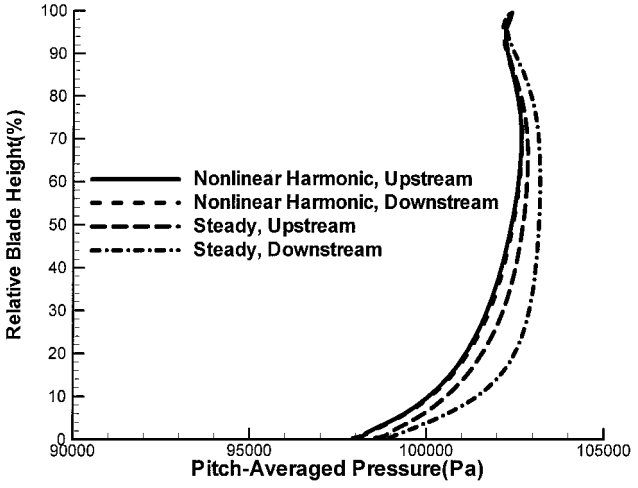

Fig. 10 Pitch-averaged pressure across the interface.

nonlinear harmonic method. Figure 11 shows a very good match of deterministic stress $(\rho u)'u'$ between the nonlinear time-marching method and the nonlinear harmonic method. In addition, Fig. 12 shows a fairly accurate match of $(\rho u)'v'$ between them. Consistent comparisons have been achieved for all of the other deterministic stresses. This demonstrates that the nonlinear harmonic method can consistently capture the effects of nonlinear unsteadiness in three-dimensional flows.

The nonlinear time-marching solution of three-dimensional unsteady viscous multistage turbomachinery flow is well recognized as being very time consuming. Even for a stage with a blade count ratio of 1:1, an unsteady time-marching calculation would typically take 15 times more CPU time than that required for the steady one.[29] In the present test case, with the first two orders of wake perturbations and the first order of potential perturbation included, the nonlinear harmonic method takes five times more CPU time than the steady method. Thus, for a stage with unit blade count ratio, the nonlinear harmonic method can be three times more efficient than a nonlinear time-marching method. Note that, for the nonlinear harmonic method, only one passage has to be calculated for each blade row, independent of the blade count ratio. However, for the nonlinear time-marching method, a multipassage (even whole annulus) domain has to be adopted. Thus, for general practical situations, the nonlinear harmonic method, although retaining most of the nonlinear effects, should be much faster than conventional nonlinear time-marching methods. The gaining factor in computational efficiency will be in proportion to the number of passages adopted in the time-marching calculations. Typically, a factor of 20 or so would be expected.

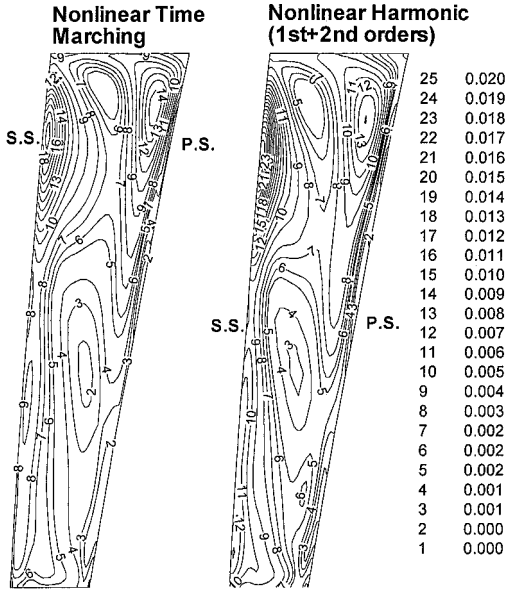

Fig. 11 Deterministic stress $\overline{(\rho u)' u'}$ on axial plane at stator midchord.

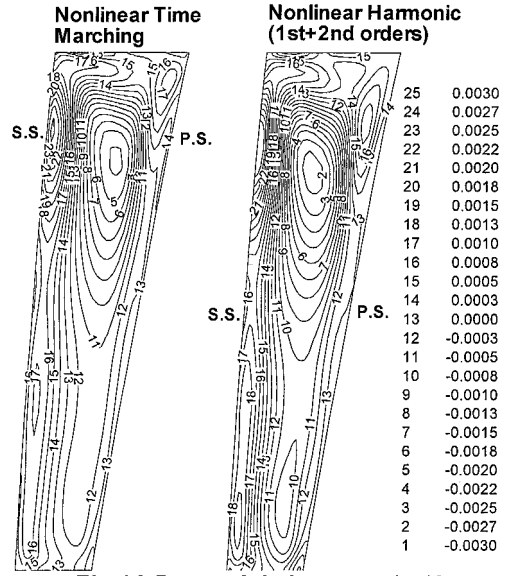

Fig. 12 Deterministic stress $\overline{(\rho u)' v'}$ on axial plane at stator midchord.

Conclusions

A new nonlinear harmonic method has been developed for aerodynamic analysis of unsteady multistage turbomachinery flows. The computed deterministic stress distributions for multirow compressor configurations are compared to those by using a fully nonlinear time-marching method. For both two-dimensional and three-dimensional compressor stage configurations, wake and deterministic stress distributions have been predicted to good agreement. With the first two orders of wake harmonic perturbations, about 90% mixing loss could be recovered at the interface. In terms of computational efficiency, the nonlinear harmonic method is about three times more efficient than a typical nonlinear time-marching calculation for a single blade-to-blade passage domain. Given that a single passage domain can always be used for the frequency-domain method, whereas a multipassage (even whole annulus) domain might have to be adopted for a conventional time-domain method, the present nonlinear harmonic method could be faster by as many as 20 times.

Acknowledgments

This work is sponsored by ALSTOM Power, Ltd. The authors would like to thank Roger Wells, Yansheng Li, and Wei Ning for their technical support.

References

[1]Erdos, J. I., Alzner, E., and Mcnally, W., "Numerical Solution of Periodic Transonic Flow Through Fan Stage," *AIAA Journal*, Vol. 15, No. 11, 1977, pp. 1559–1568.

[2]Rai, M. M., "Three-Dimensional Navier–Stokes Simulations of Turbine Rotor–Stator Interaction," *AIAA Journal*, Vol. 5, No. 3, 1989, pp. 305–319.

[3]Giles, M. B., "Stator/Rotor Interaction in a Transonic Turbine," *Journal of Propulsion and Power*, Vol. 6, No. 5, 1990, pp. 621–627.

[4]Arnone, A., and Pacciani, R., "Rotor/Stator Interaction Analysis Using the Navier–Stokes Equations and Multigrid Method," *Journal of Turbomachinery*, Vol. 118, No. 4, 1996, pp. 679–689.

[5]Dorney, D. J., and Sharma, O. P., "Evaluation of Flow Field Approximations for Transonic Compressor Stages," *Journal of Turbomachinery*, Vol. 119, No. 3, 1997, pp. 445–451.

[6]Hall, E. J., "Aerodynamic Modeling of Multistage Compressor Flowfields—Part 1: Analysis of Rotor/Stator/Rotor Aerodynamic Interaction," American Society of Mechanical Engineers, Paper 97-GT-344, 1997.

[7]Hall, E. J., "Aerodynamic Modeling of Multistage Compressor Flowfields—Part 2: Modeling Deterministic Stresses," American Society of Mechanical Engineers, Paper 97-GT-345, 1997.

[8]He, L., "An Euler Solution for Unsteady Flows Around Oscillating Blades," *Journal of Turbomachinery*, Vol. 112, No. 3, 1990, pp. 714–722.

[9]Gerolymos, G. A., "Advances in the Numerical Integration of the Three-Dimensional Euler Equations in Vibrating Cascades," *Journal of Turbomachinery*, Vol. 115, No. 4, 1993, pp. 781–790.

[10]Giles, M. B., "Calculation of Unsteady Wake/Rotor Interaction," *Journal of Propulsion and Power*, Vol. 4, No. 4, 1988, pp. 356–362.

[11]Ho, Y.-H., and Lakshminarayana, B., "Computation of Unsteady Viscous Flows Through Turbomachinery Blade Row Due to Upstream Rotor Wakes," *Journal of Turbomachinery*, Vol. 117, No. 4, 1995, pp. 541–552.

[12]Adamczyk, J. J., "Model Equations for Simulating Flows in Multistage Turbomachinery," American Society of Mechanical Engineers, Paper 85-GT-226, 1985.

[13]Adamczyk, J. J., "Aerodynamic Analysis of Multistage Turbomachinery Flows in Support of Aerodynamic Design," International Gas Turbine Inst. Scholar Lecture, American Society of Mechanical Engineers, Paper 99-GT-80, 1999.

[14]Hall, K. C., and Crawley, E. F., "Calculation of Unsteady Flows in Turbomachinery Using the Linearized Euler Equations," *AIAA Journal*, Vol. 27, No. 6, 1989, pp. 777–787.

[15]Florea, R., Hall, K. C., and Cizmas, P. G. A., "Reduced Order Modeling of Unsteady Viscous Flow in a Compressor Cascade," AIAA Paper 96-2572, 1996.

[16]Linquist, D. R., and Giles, M. B., "On the Validity of Linearized Unsteady Euler Equations with shock Capturing," AIAA Paper 91-1958, 1991.

[17]Giles, M. B., "An Approach for Multi-Stage Calculations Incorporating Unsteadiness," American Society of Mechanical Engineers, Paper 92-GT-282, 1992.

[18]He, L., "Modelling Issues for Computation of Unsteady Turbomachinery Flows," Unsteady Flows in Turbomachines, von Kármán Inst. Lecture Series 1996-05, von Kármán Inst. for Fluid Dynamics, Brussels, Belgium, 1996.

[19]Ning, W., and He, L., "Computation of Unsteady Flows Around Oscillating Blades Using Linear and Non-Linear Harmonic Euler Methods," *Journal of Turbomachinery*, Vol. 120, No. 3, 1998, pp. 508–514; also American Society of Mechanical Engineers, Paper 97-GT-229, 1997.

[20]He, L., and Ning, W., "Efficient Approach for Analysis of Unsteady Viscous Flows in Turbomachines," *AIAA Journal*, Vol. 36, No. 11, 1998, pp. 2005–2012.

[21]Baldwin, B. S., and Lomax, H., "Thin Layer Approximation and Algebratic Model for Separated Turbulent Flows," AIAA Paper 78-257, 1978.

[22]Ni, R. H., and Sisto, F., "Numerical Computation of Nonstationary Aerodynamics of Flat Plate Cascade in Compressible Flow," American Society of Mechanical Engineers, Paper 75-GT-5, 1975.

[23]Giles, M. B., "Nonreflecting Boundary Conditions for the Euler Equations," *AIAA Journal*, Vol. 28, No. 12, 1990, pp. 2050–2058.

[24]Denton, J. D., "The Calculation of Three-Dimensional Viscous Flow Through Multistage Turbomachine," *Journal of Turbomachinery*, Vol. 114, No. 1, 1992, pp. 18–26.

[25]Saxer, A. P., and Giles, M. B., "Quasi-Three-Dimensional Nonreflecting Boundary Conditions for Euler Equations Calculations," *Journal of Propulsion and Power*, Vol. 9, No. 2, 1993, pp. 263–271.

[26]Whitehead, D. S., "The Calculation of Steady and Unsteady Transonic Flow in Cascades," Dept. of Engineering, Rept. CUED/A—Turbo/TR11, Univ. of Cambridge, Cambridge, England, U.K., 1982.

[27]Dunker, R. J., "Flow Measurements in the Stator Row of a Single-Stage Transonic Axial-Flow Compressor with Controlled Diffusion Stator Blades, Paper 23, CP-351, AGARD, 1983.

[28]Fritsch, G., and Giles, M. B., "An Asymptotic Analysis of Mixing Loss," *Journal of Turbomachinery*, Vol. 117, No. 3, 1995, pp. 367–374.

[29]Graf, M. B., Greitzer, E. M., Marble, F. E., and Sharma, O. P., "Effects of Stator Pressure Field on Upstream Rotor Performance," American Society of Mechanical Engineers, Paper 99-GT-99, 1999; also *Journal of Turbomachinery* (to be published).